Contents lists available at ScienceDirect

Applied Thermal Engineering

journal homepage: www.elsevier.com/locate/ate

Highlights

The effect of micro-encapsulation on thermal characteristics of metallic phase change materials

Applied Thermal Engineering xxx (xxxx) xxx

Jingru Z. Benner, Rebecca C. Shannon, Wentao Wu, Lu Shen, Austen P. Metsack, Jingzhou Zhao*

- Encapsulation enhances convection due to the increased surface area
- Thicker shell shortens core melting time
- Heating time depends on the ratio of heat capacitance and convection rate
- Optimal shell thickness exists for achieving high energy storage and fast absorption

Contents lists available at ScienceDirect

Applied Thermal Engineering

journal homepage: www.elsevier.com/locate/ate

Research paper

The effect of micro-encapsulation on thermal characteristics of metallic phase change materials

Jingru Z. Benner [a], Rebecca C. Shannon [a], Wentao Wu [b], Lu Shen [a], Austen P. Metsack [a], Jingzhou Zhao [a,*]

[a] Department of Mechanical Engineering, Western New England University, Springfield, MA 01119, USA
[b] Department of Civil and Architectural Engineering, Tennessee State University, Nashville, TN 37209, USA

ARTICLE INFO

Keywords:
Micro-encapsulated phase change material
Encapsulation effect
High temperature thermal energy storage
Laten Heat Energy Storage
Energy Density

ABSTRACT

Micro-encapsulated phase change material with metallic core can work under high temperature for energy storage purpose, making it an appealing candidate for renewable energy technologies, such as thermal energy storage for concentrating solar power plants. The objective of this work is to study the impact of encapsulation on the thermal performance of the micro-encapsulated phase change materials under various operating conditions. To evaluate the thermal performance of the micro-encapsulated phase change material particles, the governing equation of transient heat conduction with phase change in spheres with composite walls is solved numerically. The impact of encapsulation shell on the convective heat transfer rate, total energy absorption, latent heat ratio, energy density, and duration of phase change is presented and analyzed under different operating conditions. Three different core materials including tin, aluminum and copper with distinct Stephan numbers are investigated. In addition to the encapsulation shell effect, this model can be used to study micro-encapsulated phase change materials with different material compositions, core to shell ratios, and it can be used to analyze the impact of air gaps in between materials. Understanding the thermal performance at particle level is essential, and the results of this study could potentially be used as input for thermal energy storage system level analysis, such as the charging and discharging processes.

1. Introduction

A micro-encapsulated phase change material (MEPCM) is composed of a core that is enclosed in an outer shell. When used for thermal energy storage (TES) purposes, the MEPCM core, which is the phase change material (PCM), experiences melting or vaporization to absorb latent heat, while the encapsulation shell remains in its original phase during the process. The shell helps to restrain the core in its liquid or gaseous state and keep the absorbed energy in place. Heat stored in the system can later be released through a heat exchange process and be used directly. The stored thermal energy can also be converted to a different form of energy, such as electricity. TES systems with PCMs are of great interest to renewable energy sources that are only available intermittently such as concentrating solar power (CSP) and the recovery of industrial waste heat. The added latent heat storage can improve system efficiency and further enable flexibility and stability in heat/electricity delivery rate.

The amount of latent heat absorbed and stored in PCM has drawn much attention for TES systems and research in this area has been reviewed [1] for many applications, such as thermal comfort in vehicles [2], passive energy storage in buildings to meet heating and cooling needs [3], and food transportation [4,5] etc. PCMs that are used in these applications include organic substances (paraffin wax) [6], inorganic substances (salt hydrate, water/ice) [7], and fatty acids [8], have low thermal conductivity (less than 1 W/(m K)), and most of them have a phase transition temperature below 80 °C [9]. They are not suitable to be used as CSP energy storage medium, which needs to operate at a much higher temperature. The current state of the art TES medium in CSP plants is molten salt, which delivers thermal energy at 565 °C [10]. In order to increase the energy efficiency, CSP Gen3 project in the US has expected the operating temperature to be greater than 700 °C and up to 1500 °C [11] in order to meet their 2030 cost target. The PCMs that have been considered for such high temperature applications [12–15] are metallic and alloy PCMs for their high phase transition temperature and other superior thermal properties, including high thermal conductivity and thermal capacity.

* Corresponding author.
E-mail addresses: jingru.benner@wne.edu (J.Z. Benner), jingzhou.zhao@wne.edu (J. Zhao).

https://doi.org/10.1016/j.applthermaleng.2022.118055
Received 6 July 2021; Received in revised form 3 December 2021; Accepted 5 January 2022

The objective of this work is to investigate the impact of micro-encapsulation on the thermal performance of metallic PCMs. The benefit of encapsulating metal PCMs is intuitive and well known: The containment prevents PCMs from reacting with external environments, serves as corrosion resistive barrier and supporting structure for the PCMs, and provides ease of handling. Additionally, the encapsulation increases surface area for heat transfer. Established encapsulation methods include self-assembly, coaxial electrospinning, and sol gel [16–18]. Most of these methods are designed to fabricate organic polymers that melt at lower temperature. The encapsulation of metallic PCMs was conceptualized in the 1980s [19], and recent developments in metallic PCM encapsulation including thermal oxidation [20,21], chemical vapor deposition (CVD) [22], electroplating [23], phase separation [24,25] and flow mold casting (FMC) [26] have made significant progress in the past decade, thus moving high temperature MEPCMs from research and development stage closer to applications. Along with the advancement in manufacturing, this work will fill in the knowledge gap to understand the effect of encapsulation on the thermal characteristics of MEPCM at the particle level before it can be successfully utilized in batch as TES medium at the system level. Understanding the effect of encapsulation is also of great importance for the development of certain manufacturing processes [26], during which the shell and core materials go through melting and solidification to form the MEPCM particles.

In order to study the effect of encapsulation on the thermal performance of MEPCM particles, such as energy density, absorption and release rate, one needs to solve the transient heat conduction problem that involves phase change. A considerable amount of theoretical analysis exists on heat conduction in spherical geometry [27–29], with solutions available for both steady state and transient heat conduction with different boundary conditions. When considering phase change inside of a spherical enclosure, the experimental [30,31] and numerical studies [32,33] are conducted at a larger scale (PCM is in mm$s$ or bigger) under low temperature, and the shells are very thin. The shell was either ignored justifiably or assumed to have a thermal conductivity of infinity in these studies. Since the thickness of the shell at micro-scale is comparable to the core radius, the impact of the shell in MEPCMs cannot be ignored.

To look into the encapsulation effect on the thermal performance of MEPCMs at high temperature, this paper is organized as follows. First, we present the numerical approach in the methods section to solve the transient heat conduction problem in a composite sphere with melting and solidification. The method is verified using analytical and numerical solution when applicable. The numerical model is applied to explore the encapsulation effect during energy absorption after verification. Three different PCM materials including tin, aluminum and copper with Ste number ranging low, medium, and high are evaluated, and the impact of shell thickness on energy absorption quantity and rate is discussed. Since the thermal performance of the MEPCMs is process dependent, next we show that change of parameters such as the initial temperature, heat transfer fluid flow rate and temperature will alter the ratio of the latent heat to the total energy storage during the process. Among the operating conditions, the impact of heat transfer fluid temperature and flow rate is illustrated in the content of theoretical thermal cycling that includes both melting and solidification, to demonstrate the scale of variables at particle level.

2. Methods

In this study, we assume the MEPCM particles with metal cores are exchanging energy with the surrounding fluid (the heat transfer fluid) by convection only. The shell surface is exposed to heat transfer fluid at temperature T_{HTF}, and heat transfer coefficient h. The transient heat conduction with phase change inside the particle, from the shell to the center of the core, is solved using the enthalpy formulation [34,35] of the energy equation, where the specific enthalpy $i(T)$ is added as a dependent variable in addition to temperature in the energy equation:

$$\frac{d}{dt}\int_V \rho i dV = \int_A k\nabla T d\boldsymbol{A}. \tag{1}$$

In the single phase region, the control volume V is independent of time and the integration is continuous with respect to volume and surface area. Since $i(T)$ is the product of specific heat and temperature $i(T) = c_{\mathrm{p}}T$, the enthalpy in Eq. (1) can be eliminated to obtain the conventional heat equation:

$$\rho c\frac{\partial T}{\partial t} = \nabla\cdot(k\nabla T). \tag{2}$$

In the region where both liquid and solid are present, the $i(T)$ is the sum of sensible enthalpy and latent heat. For isothermal solidification and melting, the added energy is the specific latent heat of fusion L, which is released at the melting temperature of the material:

$$i(T) = \begin{cases} c_{\mathrm{p}}T & \text{when } T < T_{\mathrm{m}} \\ c_{\mathrm{p}}T + L & \text{when } T \geq T_{\mathrm{m}}. \end{cases} \tag{3}$$

A heat source term may be derived for the core region undergoing a phase change based on the definition of enthalpy in Eq. (3):

$$S = \rho\frac{\partial(i - c_{\mathrm{p}}T)}{\partial t}, \tag{4}$$

and substitute Eq. (4) to Eq. (1) we got:

$$\frac{d}{dt}\int_V \rho c_{\mathrm{p}}T dV + S = \int_A k\nabla T d\boldsymbol{A}. \tag{5}$$

The source term S represents the rate of change of volumetric latent heat in the system. It is zero when phase change is not present, and the energy equation can be simplified shown in Eq. (2). When the system undergoes an isothermal phase change, this source term is discretized linearly using a numerical scheme detailed in [36]. One eighth of the MEPCM particle is selected as the computational domain over which Eq. (5) is solved numerically, using C++ code written in open source CFD package OpenFOAM. Symmetric boundary condition is applied on the three cut planes. The computational domain consists of a metallic core (of radius r_{c}) and a shell (of thickness th). Two interfaces exist in the computational domain. One is the geometric interface between the core and shell, which is assumed to remain in place during the process. The other is the solid and liquid state interface within the core of the MEPCM particle, which only exists during phase change and moves through the core region radially. One key encapsulation parameter, shell thickness to core radius ratio $\phi = th/r_{\mathrm{c}}$, and its impact on the thermal performance of MEPCMs with metal cores of various materials will be investigated. $\phi = 0$ refers to a case where the metal particle is not encapsulated.

It is helpful to note the range of two dimensionless variables for this study, as they provide insight of the physical phenomena. One is Biot number, which signifies the surface convection compared to the MEPCM particle internal conduction: $Bi = hr_{\mathrm{o}}/k$. The other is Stefan number, which indicates the importance of latent heat compared to sensible heat during the phase change process $Ste = c_{\mathrm{p}}|T_{\mathrm{m}} - T_{\mathrm{ref}}|/L$ [37]. The range of Biot number and Stefan number for selected core materials in this analysis is shown in Table 1. h is set to be $100 \sim 500\,\mathrm{W/(m^2\,K)}$, and the heat transfer fluid temperature surrounding the MEPCMs (T_{HTF}) is used as the reference temperature. The small Biot number ($\lesssim$0.1) suggests that the spatial temperature gradient within the metal core is

Table 1
Bi & Ste for three different core materials.

Material	T_{ref} (°C)	Bi	Ste
Sn	1500	$(15 \sim 375)\times 10^{-6}$	3.84
Al	800 ~ 1500	$(4.8 \sim 119)\times 10^{-6}$	0.31 ~ 1.32
Cu	1500	$0.3\times 10^{-6} \sim 0.0025$	0.26

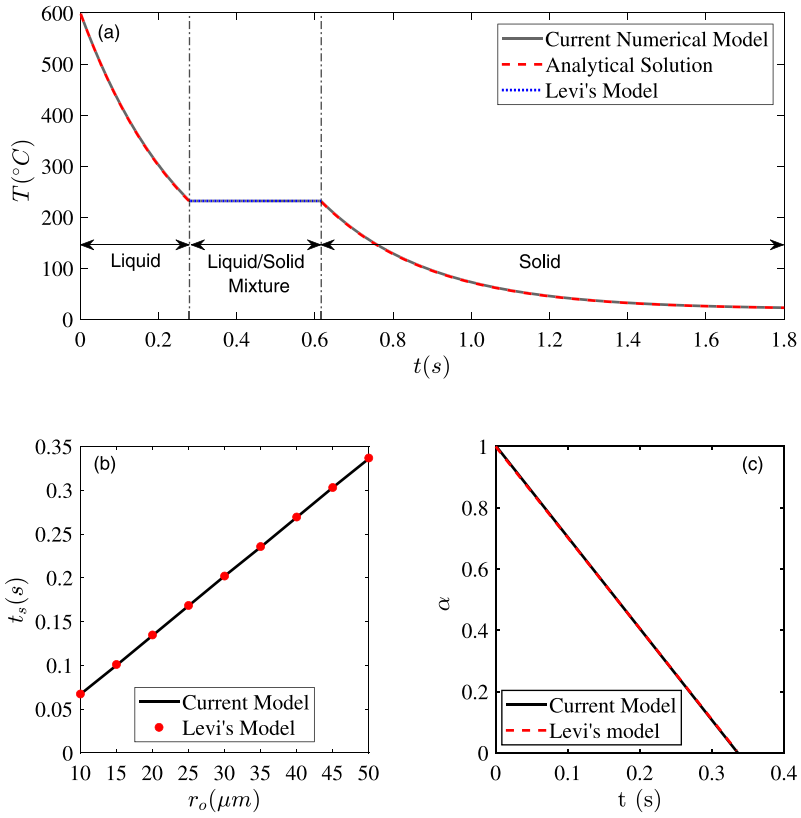

Fig. 1. Model validation. Plotted data is for MEPCM particle with Tin core, $r_c = 50\,\mu m, \phi = 0$, Bi = $1.5 \sim 7.5 \times 10^{-5}$, and Ste = 0.82. (a) Temperature history from the current numerical model, LCM and Levi's model. LCM is shown in red dashed line and only available in the sections without solidification. The duration of the isothermal solidification from Levi's model is extracted and plotted in blue dotted line. (b) The total solidification time t_s increases linearly with PCM core radius as shown in both the current model and Levi's model. (c) The change of liquid fraction α decreases linearly with time shown in both models.

negligible. It implies that lumped capacitance method (LCM) applies when Robin condition, the boundary condition of the third kind, is imposed on the computational domain. Small Stefan number means that the latent heat is the majority form of energy absorbed or released at the solid/liquid interface during the phase change process. Because T_{HTF} is used as the reference temperature, the change of the ratio of latent heat to total energy due to the change of ϕ and initial temperature T_i of the process are not reflected by values in Table 1, but they will be discussed in Section 3.

2.1. Numerical model validation

For the purpose of model validation, we separate the temperature history results obtained from the numerical model into two segments: without and with phase change. LCM is used to verify the numerical results before and after the phase change, and Levi's Newtonian method [38,39] is used to confirm the time duration of the isothermal solidification. When the internal resistance to conduction in the MEPCM particle is much less than the external convective resistance across the particle boundary layer, LCM states that transient heat conduction presented in Eq. (2) with Robin boundary condition can be rewritten by ignoring the spatial temperature distribution. This means that the rate of heat loss at the particle surface must equal to the rate of change of internal energy shown in Eq. (6).

$$\rho V c_p \frac{dT}{dt} = -hA(T - T_\infty). \tag{6}$$

The analytical solution of Eq. (6) describes the temperature history of the particle without phase change:

$$T = (T_i - T_{HTF})e^{-t/\tau_t} + T_{HTF}, \tag{7}$$

where τ_t is the thermal time constant $\tau_t = \rho V c_p / hA$.

Since both LCM and Levi's model are only for homogeneous materials, ϕ is set to be 0 for the case in Fig. 1. Core center temperature is plotted in Fig. 1a, which overlays the prediction from the current model and the LCM method (Eq. (7)) in solid line and dashed red line, respectively. The section of numerical results during which solidification happens is compared to Levi's model. His Newtonian model began with a single nucleation event occurring on the particle surface. The solid and liquid interface propagation rate is solved and correlated to particle size, the liquid and solid interface kinetic coefficient $K = (r_c/\alpha_L)(L/c_{pL})K_M$, where α_L is the thermal diffusivity of the material at liquid state, c_{pL} the specific heat at liquid state, and K_M is a kinetic parameter. K_M describes the interface velocity in the linear law at the melting temperature T_m: $K_M = -(LD_{LM}/aRT_m^2)$, where D_{LM} is the self diffusion coefficient in the liquid at T_m, a is the atom spacing, R is the gas constant. This interface velocity governed by linear growth law applied for processes with small to moderate undercooling [38,40]. Very good agreement is observed for the solidification time t_s for various particle sizes (Fig. 1b) with a root mean square error (RMSE) of 0.58 ms, and for the liquid fraction α, which tracks the liquid/solid interface propagation with time, shown in Fig. 1c with RSME of 0.0017, respectively.

The validated numerical model can expand the limits of the LCM and Levi's model. It can be used for (1) materials with non-trivial spatial temperature gradient, (2) crystalline and glassy solids, (3) sphere particles with composite walls and (4) both melting and solidification processes. The current work employs the model to study the encapsulation effect for various materials, boundary and initial conditions. The direct variables by solving Eq. (5) numerically on the computational domain are the temperature history everywhere on the MEPCM, and the time duration of the phase change t_{melt} and t_s. To study encapsulation shell effect on the thermal performance of MEPCMs, more variables are

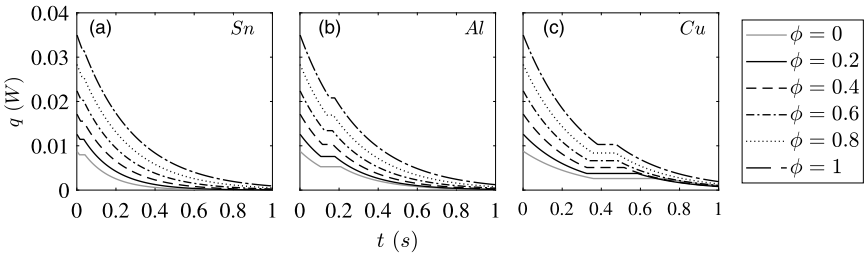

Fig. 2. q vs. t for MEPCM particle with Sn, Al, and Cu core. The core radius r_c is 50 μm, and the initial and boundary conditions are the same for all cases (T_i = 100 °C, T_{HTF} = 1500 °C, h = 200 W/(m^2 K)).

Table 2
Thermal physical properties of the MEPCM core and shell.

Material	k W/(m K)	c_p J/(kg K)	ρ kg/m^3	L kJ/kg	T_m K
Tin	66.6	228	7260	59.2	505
Aluminum	210	900	2699	386.9	933.5
Copper	401	385	8960	208.7	1357.8
Fused Silica	1.38	749	2200	2400	–[a]

[a]The melting temperature for fused silica is listed differently under various manufacturers due to chemical composition variation and form; typically above 1500 °C [41].

extracted, including the heat transfer rate q, energy density per unit volume $\dot{E}_{vol}$ and per mass $\dot{E}_{sp}$, and the ratio of latent heat to the total energy storage, referred to as latent heat ratio LHR. These variables are evaluated at different encapsulation shell thicknesses, quantified by the ratio of shell thickness and core radius ϕ.

3. Results and discussion

Three different core materials, including tin, aluminum, and copper are presented. The shell material of all MEPCM particles is set as fused silica. The relevant material properties are listed in Table 2. While the material properties offer many insights, the thermal performance of the MEPCMs is inevitably associated with the process parameters, which we will take into consideration and explore in this study.

3.1. Encapsulation effect during energy absorption

The heat transfer rate q versus ϕ during the energy absorption process is shown in Fig. 2. The boundary and initial conditions including the initial temperature T_i, heat transfer fluid temperature T_{HTF} and heat transfer coefficient h are set to be the same for all the cases in the figure. At $t = 0$, q is the same (q = 0.0088 W at $\phi = 0$, q = 0.0126 W at ϕ = 0.2, q = 0.0171 W at ϕ = 0.4, q = 0.0224 W at ϕ = 0.6, q = 0.0283 W at ϕ = 0.8, and q = 0.035 W at ϕ = 1 respectively)for all three core materials at fixed ϕ, since h and T_i are the same. The temperature of the MEPCM particle becomes higher as it absorbs energy, which effectively reduces the temperature difference between the particle and the heat transfer fluid. This leads to a decreasing q with time for each curve. The melting process is isothermal for all three selected metal cores, as indicated by the flat section on the q curve. q increases as ϕ increases, due to the added particle surface area for convection with thicker shells. As ϕ increases from 0 to 1, the surface area A_s is enlarged by 4 times, from 0.0314 mm^2 to 0.1257 mm^2. Correspondingly, the initial q is increased by 4 times, from 0.0088 to 0.035 W. The impact of increasing ϕ is the most prominent at the beginning of heating up, as q decays exponentially with time.

Intuitively, the high heat transfer rate for MEPCMs particles with thicker shells will lead to more energy absorption for one individual particle (Fig. 3a). However, in order to understand the process better and maximize the potential of MEPCMs in energy storage applications, it is important to take a closer look at the constituents of the absorbed

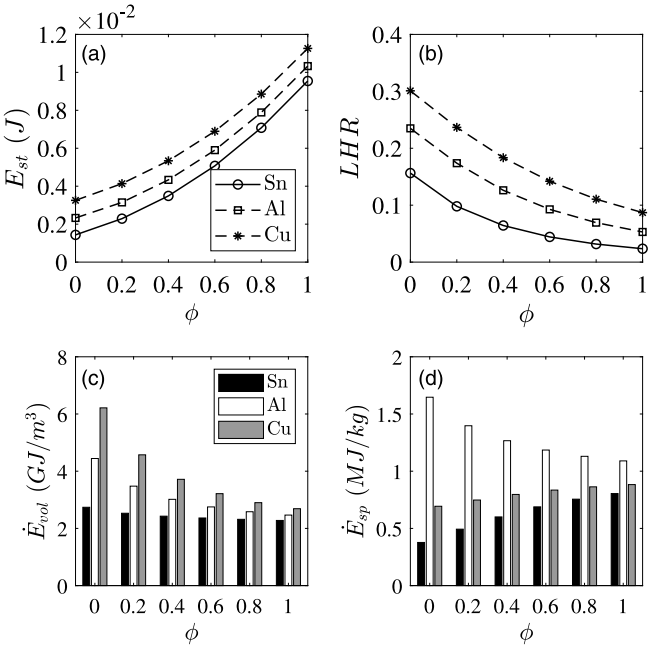

Fig. 3. Encapsulation effect on variables related to energy absorption. (a) Total energy absorption E_{st}. (b) Latent heat ratio (LHR). (c) Volumetric energy density $\dot{E}_{vol}$. (d) Specific energy $\dot{E}_{sp}$. The legends for (a) & (b) and (c) & (d) are the same; therefore they are labeled only once respectively. The initial and boundary conditions are the same as Fig. 2.

energy. The total energy stored in the particle comes from both latent and sensible heat. The ratio of latent heat to the total energy storage, LHR, decreases as ϕ increases (Fig. 3b), due to the increasing storage of the latter form of energy—sensible heat. Because the core was completely melted during the process and the total mass of core remains the same for various ϕ in this study, the latent heat absorption only depends on the intrinsic properties of the core material, including the latent heat of fusion and density (listed in Table 2). Therefore, the latent heat absorption remains unchanged for given core size and material. Since the encapsulation shell does not melt during the process, it only contributes to sensible heat addition. The LHR values in Fig. 3b indicate that the sensible heat weighs more for particles with thicker shells. Copper has the highest LHR value, varying from 0.3 at $\phi = 0$ to 0.09 at $\phi = 1$. LHR of Tin is the lowest among all three materials, with a range from 0.16 to 0.02 as ϕ increases from 0 to 1. All the LHR values are below 0.3, which indicates that given the boundary and initial conditions prescribed for cases in Fig. 2, sensible heat is the major form of energy stored within the particle.

Even though the total energy storage increases with ϕ, the total volume V_{total} of the MEPCM particle increased by 8 times from 5.24 × 10^{-13} m^3 to 4.19×10^{-12} m^3 when ϕ increases from 0 to 1, thus leading to a diminishing energy storage density per unit volume $\dot{E}_{vol}$ (Fig. 3c). The change in $\dot{E}_{vol}$ due to the added shell is the most prominent for copper,

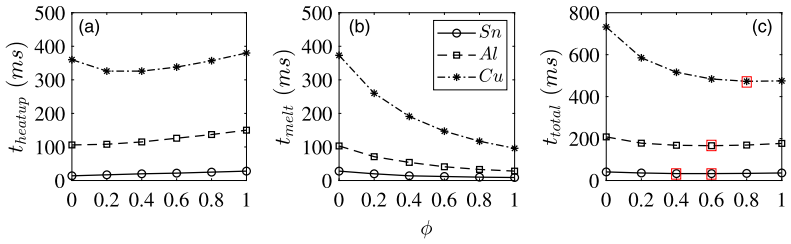

Fig. 4. (a) t_{heatup} vs. ϕ, (b) t_{melt} vs. ϕ and (c) t_{total} vs. ϕ. The initial and boundary conditions are the same as Fig. 2.

which dropped from 6.21 GJ/m^3 to 2.69 GJ/m^3 when ϕ increases from 0 to 1, representing a 57% decrease. The $\dot{E}_{\text{vol}}$ is reduced from 4.44 GJ/m^3 to 2.46 GJ/m^3 for the particle with aluminum core, which is a 45% decrease. The $\dot{E}_{\text{vol}}$ only decreased by 17% for MEPCM with tin core, from 2.74 GJ/m^3 to 2.28 GJ/m^3. This is consistent with the declining LHR trend for each material, as the sensible heat climbs up. Unlike $\dot{E}_{\text{vol}}$, the specific energy $\dot{E}_{\text{sp}}$ increases as ϕ increases for tin and copper. The $\dot{E}_{\text{sp}}$ of MEPCM with aluminum core decreases as ϕ increases, and it is noticeably larger than the other two materials due to its light weight. The low density advantage is most prominent when $\phi = 0$, at which $\dot{E}_{\text{sp}}$ is 1.64 MJ/kg for MEPCM with aluminum core, 0.69 MJ/kg for copper, and 0.38 MJ/kg for tin. At $\phi = 1$, the added shell weighs in so the difference among three different MEPCMs is smaller: 1.09 MJ/kg for aluminum, 0.88 MJ/kg for copper, and 0.80 MJ/kgfor tin. MEPCMs with high $\dot{E}_{\text{sp}}$ have the benefit of making high temperature energy storage systems more mobile and portable.

In addition to the amount of energy absorption, the other important factor is the rate of energy absorption for the MEPCM particles. Two variables of time, t_{melt} (Fig. 4a) and t_{heatup} (Fig. 4b) are used to characterize the transient process. t_{heatup} is the time that it takes to initiate the melting process of the MEPCM core, followed by t_{melt}, the duration of melting. t_{heatup} for tin and aluminum increase as ϕ increases. For MEPCM with copper core, t_{heatup} is first reduced from 360 ms ($\phi = 0$) to 326 ms ($\phi = 0.2$ & 0.4), then gradually rises to 338 ms ($\phi = 0.6$), 357 ms ($\phi = 0.8$), and 380 ms ($\phi = 1$). The change of t_{heatup} can be explained by the change of thermal time constant τ_t of the MEPCM particle, which is the product of convective thermal resistance $R_c = 1/hA_s$ and lumped thermal capacitance $C_t = \rho Vc$ of the particle. On one hand, an increase in ϕ leads to a higher C_t, causing the particle to respond slower to the change of its thermal environment. On the other hand, larger ϕ means bigger surface area, which reduces R_c of the particle. Since the increased C_t weighs more for all cases with aluminum and tin core, t_{heatup} increases monotonically. In the case of copper core, the reduction in R_c offsets the increased C_t for thinner shells ($\phi \leq 0.8$), thus causing the t_{heatup} to be shorter than the case without encapsulation.

The melting time t_{melt} decreases as ϕ increases for all cases. This aligns with the faster cooling rate with thicker shells, due to the enlarged surface area. This trend is encouraging for thermal energy storage applications, as it indicates that the encapsulation shell could lead to faster charging rate. t_{total}, the sum of t_{heatup} and t_{melt}, versus ϕ is a concave curve with minimal values boxed in red at various ϕ for different materials in Fig. 4c. At $T_i = 100$ °C, the magnitude of t_{heatup} and t_{melt} are comparable with opposite trends (Fig. 4a & b), therefore the effect of one offsets the other. It is worth pointing out that the trend of t_{total} is unique to this set prescribed initial and boundary conditions. It is practical to look into t_{heatup} and t_{melt} separately to better understand this trend. For instance, t_{heatup} will be shortened if T_i is higher, whereas t_{melt} does not vary with initial temperature. Therefore, an increasing T_{i} will diminish the weight of t_{heatup} in t_{total}. This will be further illustrated in the next section, when the initial and boundary conditions change.

3.2. Encapsulation effect under different particle $T_{\text{i}}s$

The encapsulation effect on energy density and absorption rate of MEPCM particles will vary as the operating conditions vary, including the change of initial temperature, external heat transfer fluid temperature and flow rate. To demonstrate, MEPCMs with aluminum core operating under different T_{i} is shown in Fig. 5. The rest of the parameters other than T_{i}, such as T_{HTF} and h are kept the same for all cases.

Fig. 5a shows that E_{st} decreases due to the increasing T_i as expected. As the shell becomes thicker, the difference between E_{st} at different $T_{\text{i}}s$ is enlarged. The change of the weight of latent heat in total energy is indicated by LHR shown in Fig. 5b. It decreases as ϕ increases for all different $T_{\text{i}}s$. The impact of initial temperature does not seem to be significant among different cases, particularly with thicker shells. When the thickness of the shell is the same as r_c (i.e. at $\phi = 1$), LHR is 0.14 at $T_{\text{i}} = 400$ °C and 0.20 at $T_{\text{i}} = 600$ °C. Both volumetric energy density and specific energy of the MEPCM particle decrease as ϕ and T_{i} increases (Fig. 5c & d). Although T_{i} does not affect t_{m} at fixed ϕ, Fig. 5e shows that t_{heatup} is shorter compared to t_{melt}, and the higher the T_{i}, the shorter t_{heatup} becomes. Therefore, the sum of t_{heatup} and t_{melt} decreases as T_{i} increases (Fig. 5f). Even though the elevated T_{i} accelerates the energy absorption rate indicated by t_{total}, the slope gradually becomes smaller.

3.3. Encapsulation effect under different T_{HTF} and h

The analysis presented in previous sections (Sections 3.1 and 3.2) is on energy absorption during the heating process, of which the total time is fixed at 1s, regardless of the boundary and initial conditions. TES systems usually run energy absorption, storing and releasing repeatedly, which is referred as thermal cycling. Although the duration of each process will be much longer at system level due to the added quantity of material, the operating temperature range is usually much narrower, and can be set around the MEPCM's melting temperature to maximize latent heat contribution.

Four different thermal cycling scenarios are illustrated in Fig. 6. In each scenario, the MEPCM particle with aluminum core starts at room temperature when energy absorption begins. They are exposed to hot heat transfer fluid, the temperature and heat transfer coefficient of which varies for each scenario. The energy absorption process stops when the temperature of the MEPCM core reaches to a set point, then it is immediately followed by the cooling process to release the absorbed energy, shown as the blue line segments in Fig. 6a. The heat transfer fluid is kept at 250 °C during the cooling process. The duration of energy storage period in between heating and cooling depends on the insulation package and the interval of energy demand, which is not the focus of this study. Therefore, it is left out in the scenarios. The heating and cooling process of each cycle is considered completed when the center of the MEPCM particle reaches 700 °C and 600 °C respectively. Each cycle in the scenarios is repeated three times. The results show that the process becomes periodic after the initial heating up cycle. This is due to the particle's small thermal mass. When large quantities are used for system level applications, it will take more cycles to reach thermal equilibrium and show repeatability.

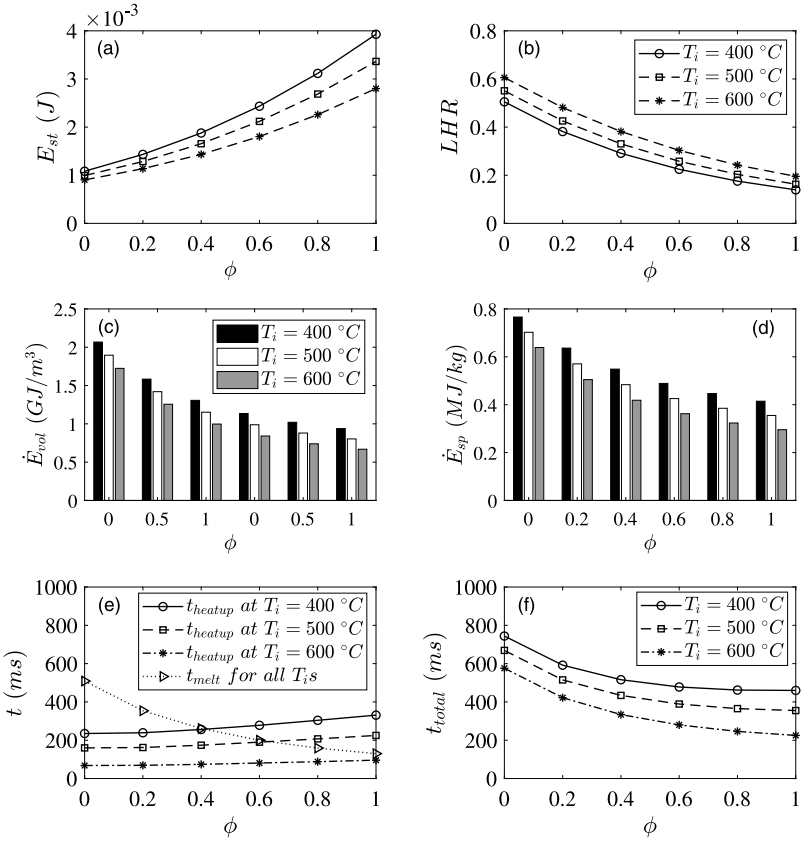

Fig. 5. Encapsulation effect at different $T_i s$ for MEPCM particle with Al core. (a) Total energy absorption in 1 s vs. ϕ, (b) LHR vs. ϕ, (c) $\dot{E}_{vol}$ vs. ϕ, (d) $\dot{E}_{sp}$ vs. ϕ, (e) t_{heatup} & t_{melt} vs. ϕ, and (f) t_{total} vs. ϕ. The boundary conditions are the same for all cases: $T_{HTF} = 1000\ ^\circ C$ and $h = 100\ W/(m^2\ K)$.

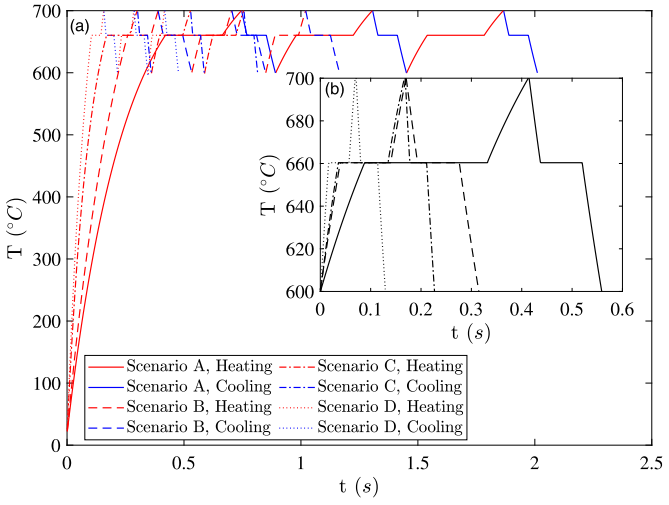

Fig. 6. Thermal cycling for MEPCMs with Al core, $\phi = 0.6$. (a) Three cycles for each scenario (one initial heat up followed by two periodic cycles). (b) One cycle for each scenario, with the starting point of the heating process aligned for all scenarios for comparison purpose. Process parameters for scenario A (solid line): $T_{HTF-HI} = 800\ ^\circ C$, $h = 200\ W/(m^2\ K)$. Scenario B (dashed line): $T_{HTF-HI} = 1000\ ^\circ C$, $h = 200\ W/(m^2\ K)$. Scenario C (dash-dotted line): $T_{HTF-HI} = 800\ ^\circ C$, $h = 500\ W/(m^2\ K)$. Scenario D (dotted line): $T_{HTF-HI} = 1000\ ^\circ C$, $h = 500\ W/(m^2\ K)$.

Fig. 6b overlays one cycle from each scenario for comparison purpose with Scenario A serving as the baseline case. Compared to Scenario A, Scenario B raised T_{HTF} during heating by 20% (from 800 °C to 1000 °C) while keeping the other process parameters the same. Scenario C keeps T_{HTF} the same as Scenario A, while increasing h from 200 to 500 W/(m^2 K). Changing h can be achieved by adjusting the heat transfer fluid properties and/or flow rate. Scenario D shows the combined effect of increasing both T_{HTF} and h. Since the MEPCM material and the peak temperatures for heating and cooling are the same for all cases, the energy absorbed per cycle for all cases is the same. Increasing T_{HTF} and h will shorten the cycles, accelerating the heating up, melting and solidification processes, which means more energy storage in 1 s. For example, the E_{st} for 1 s is increased by 76% from scenario A to B (when the T_{HTF} is raised), and it is increased by 138% from scenario A to C (when h is increased) shown in Table 3. Increasing T_{HTF} will speed up the melting process, and it has no effect on the solidification time. Increasing h in the current model setting will accelerate both the melting and solidification process. The t_{melt} and t_s decrease linearly as h increases while T_{HTF} is kept constant from Scenario A to C or B to D. The temperature history obtained from particle level analysis can potentially be used as input for thermal cycling test at system level, which needs to be performed to identify material fatigue, property degradation and structural integrity issues.

Table 3
Parameters extracted from thermal cycling scenarios in Fig. 6b.

Scenario	$E_{st} \cdot 1 \times 10^4$ J, 1s	$\dot{E}_{vol}$ GJ m^{-3}	$\dot{E}_{sp}$ MJ/kg	LHR (–)	t_{melt} μs	t_s μs
A	17	0.8	0.3	0.58	244	82
B	30	1.4	0.5	0.58	100	82
C	41	1.9	0.7	0.58	98	33
D	74	3.5	1.3	0.56	40	33

4. Conclusion

The thermal performance of MEPCM were evaluated for energy storage applications. The transient heat transfer process during which

the MEPCMs absorbs and releases sensible and latent heat is studied numerically. The impact of encapsulation on energy storage quantity and time were investigated under different initial and boundary conditions. The main conclusions are:

1. For all three core materials (tin, aluminum, and copper), increasing the encapsulation shell enhances convective heat transfer rate q due to the increased surface area.
2. As a result of the larger q, the increasing encapsulation shell also speeds up the phase change process for all materials. The temperature gradient across the shell is insignificant for MEPCMs during melting, so the rate of change of energy storage in the shell is negligible. The convective heat gain from the shell surface will directly contribute to the latent heat absorption, and lead to shorter t_{melt}.
3. Results show that for Sn and Al, the time leading up to melt t_{heatup} is longer as ϕ increases. The trend for t_{heatup} is different for copper: t_{heatup} drops at $\phi = 0.2$, then slowly increases as ϕ increases. Compared to a copper sphere without shell ($\phi = 0$), t_{heatup} is shortened in all cases with shell except for $\phi = 1$. The difference in thermal response for different materials can be explained by the ratio of the effective heat capacitance and the convective heat transfer on the surface of the MEPCM particle.
4. Although the total energy transferred increases because of the increasing ϕ, the absorbed energy per unit volume decreases with increasing ϕ, due to (i) the increased shell volume, (ii) the encapsulation shell must remain in solid state for containment purpose, therefore, it does not release latent heat in the system, (iii) the thermal capacitance of fused silica shell is smaller than all three core materials tested.

The encapsulation shell effect on energy absorption quantity and rate for MEPCM particles are presented in this study. The results indicate that an optimal shell thickness exists for achieving high energy storage and fast absorption. This particle level study paves groundwork for next generation TES system level analysis, with various design constraints, including the heat transfer fluid temperature, flow rate, storage tank size etc. Further, the results are instructive for manufacturing to tune process parameters in order to produce MEPCMs with targeted thermal characteristics that are tailored for a set of operating conditions. Lastly, the numerical approach in this work can be used to study the impact of a void between the shell and core, which is a very important attribute for composite materials.

Declaration of competing interest

The authors declare that they have no known competing financial interests or personal relationships that could have appeared to influence the work reported in this paper. Jingzhou Zhao reports financial support was provided by US Department of Energy.

Acknowledgments

The authors would like to thank John Goodhue, Julie Ma, and Josh Bevan for computational infrastructure maintenance and support. This material is based upon work supported by the U.S. Department of Energy, Office of Energy Efficiency & Renewable Energy under award number DE-EE0009095. This work used computational resources provided by the Northeast Cyberteam project funded by the National Science Foundation at the Massachusetts Green High Performance Computing Center and the Boston University Shared Computing Cluster.

References

[1] K. Reddy, V. Mudgal, T. Mallick, Review of latent heat thermal energy storage for improved material stability and effective load management, J. Energy Storage 15 (2018) 205–227, http://dx.doi.org/10.1016/j.est.2017.11.005.

[2] H. Nazir, M. Batool, F.J.B. Osorio, M. Isaza-Ruiz, X. Xu, K. Vignarooban, P. Phelan, Inamuddin, A.M. Kannan, Recent developments in phase change materials for energy storage applications: A review, Int. J. Heat Mass Transfer 129 (2019) 491–523, http://dx.doi.org/10.1016/j.ijheatmasstransfer.2018.09.126.

[3] A. Chauhan, V.V. Tyagi, S. Anand, A.K. Pandey, A. Sari, F.A. Al-Sulaiman, in: R. Wang, X. Zhai (Eds.), Energy Storage by PCM for Building Applications, Springer Berlin Heidelberg, Berlin, Heidelberg, 2018, pp. 995–1023, http://dx.doi.org/10.1007/978-3-662-49120-1_41.

[4] J.H. Johnston, J.E. Grindrod, M. Dodds, K. Schimitschek, Composite nanostructured calcium silicate phase change materials for thermal buffering in food packaging, Curr. Appl. Phys. 8 (3) (2008) 508–511, http://dx.doi.org/10.1016/j.cap.2007.10.059, AMN-3 (Third International Conference on Advanced Materials and Nanotechnology).

[5] Y. Lu, W. Zhang, P. Yuan, M. Xue, Z. Qu, W. Tao, Experimental study of heat transfer intensification by using a novel combined shelf in food refrigerated display cabinets (experimental study of a novel cabinets), Appl. Therm. Eng. 30 (2) (2010) 85–91, http://dx.doi.org/10.1016/j.applthermaleng.2008.10.003.

[6] F. Kleiner, K. Posern, A. Osburg, Thermal conductivity of selected salt hydrates for thermochemical solar heat storage applications measured by the light flash method, Appl. Therm. Eng. 113 (2017) 1189–1193, http://dx.doi.org/10.1016/j.applthermaleng.2016.11.125.

[7] A. Sarı, A. Karaipekli, Thermal conductivity and latent heat thermal energy storage characteristics of paraffin/expanded graphite composite as phase change material, Appl. Therm. Eng. 27 (8) (2007) 1271–1277, http://dx.doi.org/10.1016/j.applthermaleng.2006.11.004.

[8] A. Al-Ahmed, A. Sarı, M.A.J. Mazumder, B. Salhi, G. Hekimoğlu, F.A. Al-Sulaiman, Inamuddin, Thermal energy storage and thermal conductivity properties of fatty acid/fatty acid-grafted-CNTs and fatty acid/CNTs as novel composite phase change materials, Sci. Rep. 10 (1) (2020) 15388, http://dx.doi.org/10.1038/s41598-020-71891-1.

[9] P. Tatsidjodoung, N. Le Pierrès, L. Luo, A review of potential materials for thermal energy storage in building applications, Renew. Sustain. Energy Rev. 18 (2013) 327–349, http://dx.doi.org/10.1016/j.rser.2012.10.025.

[10] M. Mehos, C. Turchi, J. Vidal, M. Wagner, Z. Ma, C. Ho, W. Kolb, C. Andraka, A. Kruizenga, Concentrating Solar Power Gen3 Demonstration Roadmap, Tech. rep., Research Org.: National Renewable Energy Lab. (NREL), Golden, CO (United States), United States, 2017, http://dx.doi.org/10.2172/1338899.

[11] U. Pelay, L. Luo, Y. Fan, D. Stitou, M. Rood, Thermal energy storage systems for concentrated solar power plants, Renew. Sustain. Energy Rev. 79 (2017) 82–100, http://dx.doi.org/10.1016/j.rser.2017.03.139.

[12] A. Sharma, V. Tyagi, C. Chen, D. Buddhi, Review on thermal energy storage with phase change materials and applications, Renew. Sustain. Energy Rev. 13 (2) (2009) 318–345, http://dx.doi.org/10.1016/j.rser.2007.10.005.

[13] J.M. Mahdi, E.C. Nsofor, Solidification enhancement of PCM in a triplex-tube thermal energy storage system with nanoparticles and fins, Appl. Energy 211 (2018) 975–986, http://dx.doi.org/10.1016/j.apenergy.2017.11.082.

[14] S. Ramakrishnan, X. Wang, J. Sanjayan, Effects of various carbon additives on the thermal storage performance of form-stable PCM integrated cementitious composites, Appl. Therm. Eng. 148 (2019) 491–501, http://dx.doi.org/10.1016/j.applthermaleng.2018.11.025.

[15] C. Zhang, M. Yu, Y. Fan, X. Zhang, Y. Zhao, L. Qiu, Numerical study on heat transfer enhancement of PCM using three combined methods based on heat pipe, Energy 195 (2020) 116809, http://dx.doi.org/10.1016/j.energy.2019.116809.

[16] A. Jamekhorshid, S. Sadrameli, M. Farid, A review of microencapsulation methods of phase change materials (PCMs) as a thermal energy storage (TES) medium, Renew. Sustain. Energy Rev. 31 (2014) 531–542, http://dx.doi.org/10.1016/j.rser.2013.12.033.

[17] J.T. McCann, M. Marquez, Y. Xia, Melt coaxial electrospinning: a versatile method for the encapsulation of solid materials and fabrication of phase change nanofibers, Nano Lett. 6 (12) (2006) 2868–2872, http://dx.doi.org/10.1021/nl0620839.

[18] L.-Y. Wang, P.-S. Tsai, Y.-M. Yang, Preparation of silica microspheres encapsulating phase-change material by sol-gel method in O/W emulsion, J. Microencapsul. 23 (1) (2006) 3–14, http://dx.doi.org/10.1080/02652040500286045.

[19] M.R. Bennett, J. Braunstein, Hypereutectic heat storage alloy: Final report, Silicon shell integrity in molten Al-Si eutectic.

[20] N. Sheng, C. Zhu, G. Saito, T. Hiraki, M. Haka, Y. Hasegawa, H. Sakai, T. Akiyama, T. Nomura, Development of a microencapsulated al–si phase change material with high-temperature thermal stability and durability over 3000 cycles, J. Mater. Chem. A 6 (2018) 18143–18153, http://dx.doi.org/10.1039/C8TA04708A.

[21] T. Nomura, C. Zhu, N. Sheng, G. Saito, T. Akiyama, Microencapsulation of metal-based phase change material for high-temperature thermal energy storage, Sci. Rep. 5 (1) (2015) 9117, http://dx.doi.org/10.1038/srep09117.

[22] F. Zhang, Y. Zhong, X. Yang, J. Lin, Z. Zhu, Encapsulation of metal-based phase change materials using ceramic shells prepared by spouted bed CVD method, Solar Energy Mater. Solar Cells 170 (2017) 137–142, http://dx.doi.org/10.1016/j.solmat.2017.05.061.

[23] G. Zhang, J. Li, Y. Chen, H. Xiang, B. Ma, Z. Xu, X. Ma, Encapsulation of copper-based phase change materials for high temperature thermal energy storage, Solar Energy Mater. Solar Cells 128 (2014) 131–137, http://dx.doi.org/10.1016/j.solmat.2014.05.012.

[24] H. Sugo, E. Kisi, D. Cuskelly, Miscibility gap alloys with inverse microstructures and high thermal conductivity for high energy density thermal storage applications, Appl. Therm. Eng. 51 (1–2) (2013) 1345–1350, http://dx.doi.org/10.1016/j.applthermaleng.2012.11.029.

[25] Q. Zou, J. Jie, Z. Shen, N. Han, T. Li, A new concept of al-si alloy with core-shell structure as phase change materials for thermal energy storage, Mater. Lett. 237 (2019) 193–196, http://dx.doi.org/10.1016/j.matlet.2018.11.103.

[26] J. Zhao, M. Martel, Y. Gulak, Apparatus and method for production and encapsulation of small particles and thin wires, 2020, U.S. Patent US16/583, 710.

[27] J. Crank, J. Crank, Free and Moving Boundary Problems, in: Oxford science publications, Clarendon Press, 1984.

[28] J.H. VanSant, Conduction Heat Transfer Solutions, Tech. rep., Lawrence Livermore National Laboratory.

[29] H.S. Carslaw, J. Jaeger, Conduction of Heat in Solids, Oxford University Press, 1959.

[30] C. Chan, F. Tan, Solidification inside a sphere—an experimental study, Int. Commun. Heat Mass Transf. 33 (3) (2006) 335–341, http://dx.doi.org/10.1016/j.icheatmasstransfer.2005.10.010.

[31] E. Assis, G. Ziskind, R. Letan, Numerical and experimental study of solidification in a spherical shell, J. Heat Transf. 131 (2) (2008) http://dx.doi.org/10.1115/1.2993543, 024502.

[32] J. Nazzi Ehms, R. De César Oliveski, L. Oliveira Rocha, C. Biserni, Theoretical and numerical analysis on phase change materials (PCM): A case study of the solidification process of erythritol in spheres, Int. J. Heat Mass Transf. 119 (2018) 523–532, http://dx.doi.org/10.1016/j.ijheatmasstransfer.2017.11.124.

[33] A.R. Archibold, M.M. Rahman, J. Gonzalez-Aguilar, D.Y. Goswami, E.K. Stefanakos, M. Romero, Phase change and heat transfer numerical analysis during solidification on an encapsulated phase change material, Energy Procedia 57 (2014) 653–661, http://dx.doi.org/10.1016/j.egypro.2014.10.220, 2013 ISES Solar World Congress.

[34] N. Shamsundar, E.M. Sparrow, Analysis of multidimensional conduction phase change via the enthalpy model, J. Heat Transf. 97 (3) (1975) 333–340, http://dx.doi.org/10.1115/1.3450375.

[35] A.D. Brent, V.R. Voller, K. Reid, Enthalpy-porosity technique for modeling convection-diffusion phase change: Application to the melting of a pure metal, Numer. Heat Transfer 13 (3) (1988) 297–318, http://dx.doi.org/10.1080/10407788808913615.

[36] V. Voller, C. Prakash, A fixed grid numerical modelling methodology for convection-Diffusion Mushy Region phase-change problems, Int. J. Heat Mass Transf. 30 (8) (1987) 1709–1719, http://dx.doi.org/10.1016/0017-9310(87)90317-6.

[37] M.N. Ã-zisik, M.N. Özışık, M.N. Özısık, Heat conduction, John Wiley & Sons, 1993.

[38] C.G. Levi, R. Mehrabian, Heat flow during rapid solidification of undercooled metal droplets, Metallur. Trans. A 13 (2) (1982) 221–234, http://dx.doi.org/10.1007/BF02643312.

[39] J.Z. Benner, R.C. Shannon, W. Wu, A.P. Metsack, L. Shen, J. Zhao, The encapsulation effect on thermal performance of micro-encapsulated phase change materials during energy absorption, in: ASME International Mechanical Engineering Congress and Exposition, 2021.

[40] J.W. Cahn, W. Hillig, G. Sears, The molecular mechanism of solidification, Acta Metall. 12 (12) (1964) 1421–1439, http://dx.doi.org/10.1016/0001-6160(64)90130-0.

[41] G. Wypych, 2 - Fillers – origin, chemical composition, properties, and morphology, in: Handbook of Fillers, 4th ed., ChemTec Publishing, 2016, pp. 13–266, http://dx.doi.org/10.1016/B978-1-895198-91-1.50004-X.